

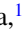
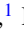




Influence of epitaxial strain on the perpendicular magnetic anisotropy of Fe/MgO systemsMasanobu Shiga ¹, Shoya Sakamoto ¹, Takaya Tsujikawa ¹, Ryoya Ando ¹, Kenta Amemiya ², and Shinji Miwa ^{1,3,*}¹*The Institute for Solid State Physics, The University of Tokyo, Chiba 277-8581, Japan*²*Institute of Materials Structure Science, KEK, Ibaraki 305-0801, Japan*³*Trans-scale Quantum Science Institute, The University of Tokyo, Tokyo 113-0033, Japan*

(Received 28 June 2021; revised 8 September 2021; accepted 1 October 2021; published 14 October 2021; corrected 2 November 2021)

Perpendicular magnetic anisotropy (PMA) in ferromagnet/oxide systems has attracted considerable attention owing to its significant potential in spintronic applications; however, an understanding of the causes of PMA enhancement in such systems remains inadequate. This study investigates the influence of epitaxial strain on PMA in the Fe/MgO system. The PMA energy increases monotonically as the in-plane lattice constant of Fe decreases, and increases further after annealing. We find that the interface component of the PMA energy is largely unaffected by the epitaxial strain and annealing process, and that changes in its bulk component play an important role. This study leads to a comprehensive understanding of PMA and voltage-controlled magnetic anisotropy effects in ultrathin magnetic films.

DOI: [10.1103/PhysRevB.104.L140406](https://doi.org/10.1103/PhysRevB.104.L140406)

Atoms in magnetic interfaces or surfaces may possess perpendicular magnetic anisotropy (PMA) owing to their lowered crystal symmetry [1–3]. In particular, the PMA that emerges at ferromagnet/oxide interfaces has been intensively investigated [4–11] as these relatively simple systems can be used in magnetic random access memory applications [12]. Among various ferromagnet/oxide systems, Fe/MgO-based systems are particularly important in applications [4,7–9] because they exhibit a significant tunneling magnetoresistance [13,14]. The microscopic origin of PMA in Fe/MgO-based systems is attributed to an enhanced orbital angular momentum due to the hybridization of O- p_z and Fe- d_{z^2} orbitals [7].

In several previous studies, thermal annealing was employed to enhance PMA energy [6,9,10,15,16]; however, it is not evident how this process modulates the interfacial structure or how the changes in PMA energy arise. Moreover, the effect of thermal annealing on the electric field induced change in PMA energy, termed the voltage-controlled magnetic anisotropy (VCMA) effect, is not significant [17,18]. It has also been reported that underlayer [16,19] and MgO overlayer [15] have significantly modulated PMA and VCMA in CoFeB films. Because these under- and overlayers are not in direct contact with the CoFeB/MgO interface, the stress in the CoFeB layer and/or CoFeB/MgO interface could be correlated to the PMA energy [20]. Although the influence of stress on the bulk contribution to the PMA energy was studied previously (cf. (Fe/V) $_n$ superlattices [21–23]), studies on the interface contribution remain elusive. As mentioned above, the origins of PMA and its enhancement after annealing remain less understood, limiting the scope of designing alternative systems with large PMA for practical applications. To this end, the present study aims to clarify the influence of thermal annealing and stress on PMA. We focused on the role

of internal stress on PMA in ultrathin ferromagnetic films, and studied a fully epitaxial MgO/V/Fe multilayer with varying epitaxial strain in the V layer. As compared to the Fe layer grown directly on MgO [24,25], the V underlayer makes it possible to characterize the influence of epitaxial strain on the magnetic properties of an ultrathin Fe film (<1 nm). We found that epitaxial strain mainly modulates the bulk PMA but negligibly affects the interface contribution to the PMA energy. The present findings are useful to understand PMA in order to design ferromagnet/oxide systems.

A fully epitaxial multilayer comprising MgO (5 nm)/V ($t_v = 6–100$ nm)/Fe ($t_{Fe} = 0.6–1.0$ nm)/MgO (2 nm)/cap was grown on single-crystal MgO(001) substrates by molecular beam epitaxy under ultrahigh vacuum. A vanadium underlayer was used to induce epitaxial strain in the ultrathin Fe layer and to achieve a large PMA without thermal annealing [8]. Moreover, in comparison to other transition metal underlayers (cf. Ag, Au, and Pd [26,27]), V segregation into Fe is believed to be negligible. The cap layer comprised either V (3 nm)/Au (3 nm), or SiO₂ (5 nm). A schematic of the sample structure is illustrated in Fig. 1(a). The MgO substrate was annealed at 800 °C for 10 min before deposition and a 5 nm thick MgO layer was grown on the substrate (at a rate of 0.1 Å/s) to avoid the diffusion of carbon atoms from the substrate into the metal films [28]. A V layer was grown at a rate of 0.2 Å/s, and the sample was annealed at 500 °C for 20 min to ensure the formation of a flat surface. Subsequently, a wedged Fe layer was deposited at a rate of 0.05 Å/s, and a 2 nm thick top MgO layer was grown at a rate of 0.1 Å/s. All the layers were deposited at room temperature. To release the epitaxial strain of the ultrathin Fe, thermal annealing was performed at 350 °C for 30 min under ultrahigh vacuum.

As depicted in Fig. 1(b), clear streak patterns were observed by reflection high-energy electron diffraction (RHEED), confirming the formation of epitaxial layers with flat interfaces. The distance between the streaks in the V

*miwa@issp.u-tokyo.ac.jp

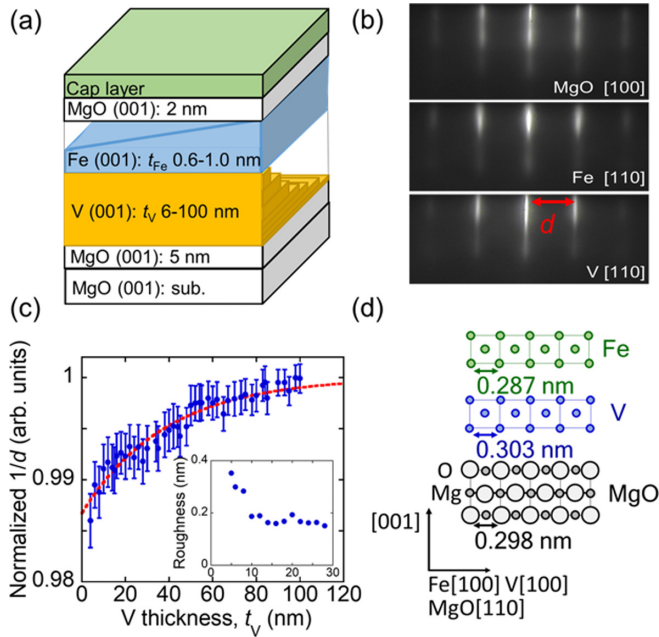


FIG. 1. (a) Schematic of the sample structure. (b) *In situ* reflection high-energy electron diffraction (RHEED) images of the V, Fe, and top MgO layers. (c) $1/d$ as a function of V layer thickness. The variable d corresponds to the distance between the streaks in the V layer RHEED image, as shown in (b). The dashed line was fitted using an exponential function. The relaxation length of the epitaxial strain was estimated as 39 nm. Inset: Root mean square surface roughness of V layer as a function of its thickness. (d) Schematic of the lattice structure of the Fe, V, and MgO layers.

RHEED image [denoted as d in Fig. 1(b)] varies with V layer thickness. Figure 1(c) depicts the V layer thickness dependence of $1/d$, with $1/d$ increasing with layer thickness. As $1/d$ corresponds to an in-plane lattice constant, this result indicates that the lattice constant of the V underlayer increases with its thickness. The observed thickness dependence of the in-plane lattice constant of the V underlayer can be understood by considering the epitaxial strain from the MgO substrate. As illustrated in Fig. 1(d), the lattice constant of V is 1.7% larger than that of MgO, which is consistent with the change in the in-plane lattice constant of the V underlayer [Fig. 1(c)]. We evaluated the surface roughness of the V layer using atomic force microscopy and found that the roughness is nearly constant beyond a thickness of 10 nm, as shown in the inset of Fig. 1(c). The results indicate that the in-plane lattice constant is successfully modulated while maintaining the film surface flat.

We estimated the magnetic dead layer in the V (30 nm)/Fe (t_{Fe})/MgO (2 nm)/SiO₂ (5 nm) sample. The inset of Fig. 2(a) illustrates the typical magnetization curve of the sample with $t_{\text{Fe}} = 0.42$ nm measured using the polar magneto-optical Kerr effect (MOKE). Square-shaped magnetic hysteresis loops were observed under a perpendicular magnetic field (H), indicating the existence of PMA in the film. The saturation Kerr rotation angle was defined as the angle at $H = 0$ Oe. The dependence of the saturation Kerr rotation angle on the thickness of Fe is shown in Fig. 2(a). In the MOKE experiment, a 660 nm wavelength light source was deployed. Since the

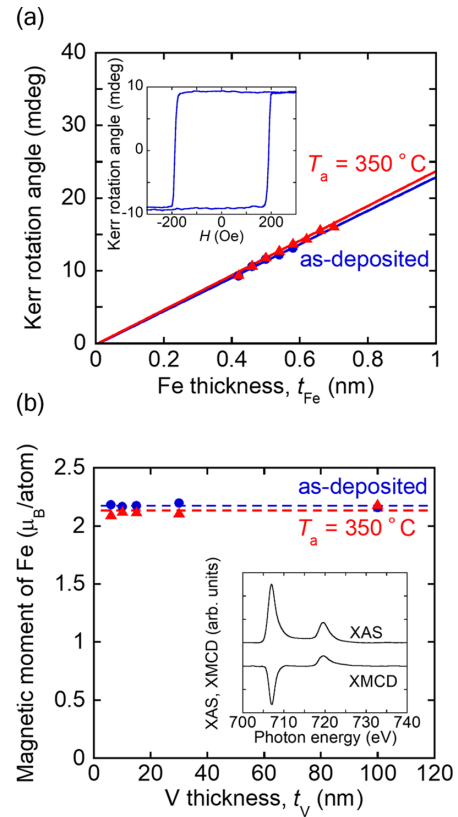


FIG. 2. (a) Saturation Kerr rotation angle as a function of Fe film thickness. The solid lines are fits using linear functions. Inset: Typical MOKE signal of the as-deposited sample with V and Fe layer thicknesses of 30 nm and 0.42 nm, respectively. An external magnetic field was applied normal to the sample surface. (b) Magnetic moment of Fe shown as a function of V layer thickness. The dashed line is the average value of the experimental data. Inset: Typical XAS and XMCD spectra of the as-deposited sample with V and Fe layer thicknesses of 6 and 0.5 nm, respectively. External magnetic fields of ± 0.1 T were applied normal to the sample surface.

penetration length of its light is considerably larger than the ultrathin Fe layer thickness, the saturation Kerr rotation angle is expected to increase linearly with the layer thickness. The linear fit crosses zero near 0.01 nm for both as-deposited and annealed samples, suggesting that the magnetic dead layer is extremely thin (~ 0.01 nm). A significant magnetic dead layer (~ 0.3 nm) was previously reported in a similar V/Fe/MgO system [8]. The thickness of the magnetic dead layer increased significantly when the annealing temperature was greater than 450 °C. Hence we have used an annealing temperature of 350 °C in this study.

The impact of the V thickness on the magnetic moment of Fe was investigated. The Fe magnetic moment in our samples was estimated by performing x-ray magnetic circular dichroism (XMCD) spectroscopy at room temperature. The measurements were conducted at the BL-7A beamline of the Photon Factory, High Energy Accelerator Research Organization (KEK) [29]. A magnetic field of 0.1 T was applied normal to the sample surface to saturate the magnetization. The XMCD measurements were performed on the V (t_{V})/Fe (0.5 nm)/MgO (2 nm) samples. The x-ray absorption and

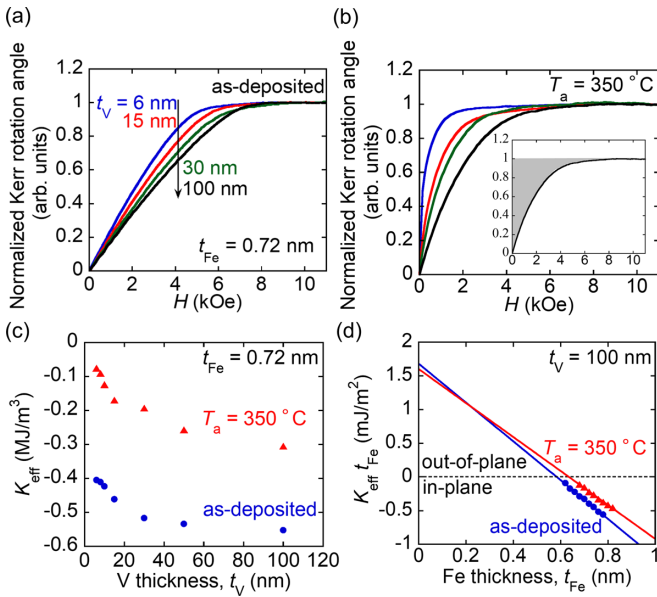


FIG. 3. (a), (b) Magnetization curves of as-deposited and annealed samples with varying V layer thickness. Inset of panel (b): Magnetization curve of the annealed sample with a thick V underlayer ($t_V = 100$ nm). The PMA energy, K_{eff} , was estimated from the shaded area. (c) The PMA energy as a function of V layer thickness. (d) The PMA energy multiplied by Fe layer thickness as a function of Fe layer thickness. The solid lines represent the fits using Eq. (1).

XMCD spectra of the sample with $t_V = 6$ nm are depicted in the inset of Fig. 2(b). By applying the sum rules [30,31], we evaluated the magnetic moments of Fe, as shown in Fig. 2(b). In both as-deposited and annealed samples, the magnetic moment of Fe was not significantly correlated to the V layer thickness. Thus we conclude that the influence of epitaxial strain on the Fe magnetic moment is negligible. As indicated by the dashed line in Fig. 2(b) representing the average experimental value, we estimated the magnetic moment of Fe in as-deposited and annealed samples to be 2.17 and 2.13 μ_B/atom , respectively. These values are close to the literature value of the bulk Fe moment (2.2 μ_B/atom) [32], implying that interdiffusion across the V/Fe interface can be neglected in both as-deposited and annealed samples.

Figure 3(a) shows the typical magnetization loops of the as-deposited samples with varying V layer thickness under out of plane magnetic fields. All the samples have an in-plane magnetized Fe film of $t_{\text{Fe}} = 0.72$ nm. For Figs. 3 and 4, a multilayer comprising V(t_V)/Fe(t_{Fe})/MgO (2 nm)/V (3 nm)/Au (3 nm) was used. The magnetic field strength required to saturate the magnetization decreases with decreasing V layer thickness, as shown in Fig. 3(a). This suggests an enhancement of the PMA energy. A similar correlation was also obtained in the annealed samples, as shown in Fig. 3(b). The PMA energy K_{eff} was calculated from the magnetization curve [shaded area in inset of Fig. 3(b)] and the saturated magnetization estimated by XMCD experiments. Figure 3(c) shows the V layer thickness dependence of K_{eff} . A positive K_{eff} value represents an out of plane magnetic easy axis, and conversely a negative K_{eff} signifies an in-plane magnetic easy axis. As the V layer thickness decreases, K_{eff} monotonically

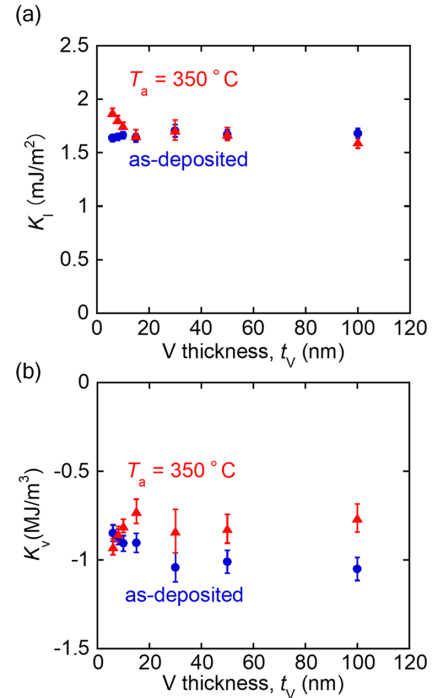


FIG. 4. (a) Interfacial anisotropy energy K_i and (b) volume anisotropy energy K_V as a function of V layer thickness.

increases. This behavior was observed in both as-deposited and annealed samples. Furthermore, thermal annealing results in an increase in K_{eff} regardless of the V layer thickness.

To separately characterize the interface (K_i) and bulk (K_V) contributions to the PMA energy, the impact of Fe layer thickness on K_{eff} was investigated. In general, these physical quantities possess the following relation, $K_{\text{eff}} = K_V + K_i/t_{\text{eff}} - 1/2\mu_0 M_S^2$, where t_{eff} and μ_0 represent the effective Fe film thickness and the vacuum permeability, respectively. The effective thickness is defined as the nominal thickness of Fe (t_{Fe}) minus the thickness of the magnetic dead layer. In this study, because the magnetic dead layer is considerably small (<0.01 nm), the effective thickness of Fe is nearly identical to the nominal thickness ($t_{\text{eff}} \approx t_{\text{Fe}}$).

$$K_{\text{eff}} t_{\text{Fe}} = \left(K_V - \frac{1}{2} \mu_0 M_S^2 \right) t_{\text{Fe}} + K_i. \quad (1)$$

From Eq. (1), K_V and K_i can be extracted as the slope and vertical intercept of the linear fit, respectively. Figure 3(d) shows the typical results of plotting $K_{\text{eff}} t_{\text{Fe}}$ as a function of Fe thickness.

Figures 4(a) and 4(b) show the interface (K_i) and bulk (K_V) contributions to the PMA energy (K_{eff}) as a function of V layer thickness. For the as-deposited samples, K_i is less affected by the V layer thickness and is estimated to be ~ 1.7 mJ/m². This is larger than the reported value of ~ 1.0 mJ/m² in V/Fe/MgO [8]. Similarly, annealing was not found to significantly change K_i . However, this is not the case for K_V , as shown in Fig. 4(b). The negative (in-plane) K_V can be attributed to the shape magnetic anisotropy and magnetocrystalline anisotropy originating from an epitaxial strain in the V underlayer. Interestingly, the in-plane magnetic anisotropy energy (negative values of K_V) strongly depends on the V layer thickness and decreases with decreasing V

layer thickness, which is consistent with the previously observed decreasing in-plane lattice constant with decreasing V layer thickness [Fig. 1(c)]. Here, decreasing the in-plane lattice constant decreases (increases) the tensile (compressive) strain of Fe (V). Using the in-plane lattice expansion of V [1.2% from Fig. 1(c)], the magnetoelastic coupling constant of Fe is estimated to be -17 MJ/m^3 , which is five times larger than that of bulk Fe (-3.4 MJ/m^3). Similar enhancement was also reported in ultrathin Co films [33]. After annealing, the in-plane magnetic anisotropy from K_V is reduced and the V layer thickness dependence is suppressed. This can be rationalized by considering the relaxation of the epitaxial strain during the thermal annealing process. The relaxation of the epitaxial tensile strain results in the in-plane lattice constant of the ultrathin Fe layer being comparable to that of bulk Fe. These observations indicate that the in-plane lattice constant for Fe decreases during thermal annealing, thus reducing the in-plane magnetic anisotropy from Fe bulk. As a result, the influence of the V underlayer on the PMA energy is suppressed. In Figs. 4(a) and 4(b), the changes in K_i and K_V for $t_V < 10\text{ nm}$ cannot be rationalized by the release of epitaxial strain. This could be due to the imperfectness of the sample. In fact, surface roughness increases in the same region ($t_V < 10\text{ nm}$) as shown in the inset of Fig. 1(c).

It is evident from Figs. 4(a) and 4(b) that the V layer thickness and annealing dependencies of the PMA energy [Fig. 3(c)] were found to originate primarily from the volume magnetic anisotropy induced by epitaxial strain. The interface contribution to the PMA energy from Fe/MgO is less affected by both epitaxial strain and annealing. This might be because the contribution is determined locally by a hybridized Fe-O bond [7] and is less affected by the in-plane Fe-Fe bond. However, the results presented herein seem inconsistent with previous studies, wherein annealing often enhances the interfacial PMA energy in Fe(CoB)/MgO-based systems [6,9,10,15,16].

For instance, in the case of the CoFeB/MgO system [6,15,16], the interfacial PMA energy was enhanced by annealing, presumably due to diffusion of B atoms [34,35]. The diffusion promotes crystallization near the CoFe(B)/MgO interface and consequently modulates the interfacial PMA energy. The enhancement of the interfacial PMA energy was also reported in the Cr/Fe/MgO system [9]. In this case, the enhancement is associated with an increase in the orbital magnetic moment anisotropy of Fe [36]. However, it has been reported that a large PMA energy at the Cr/Fe/MgO interface

is related to the dispersion of Cr atoms in the Fe layer [37,38]. Thus, the reported enhancement of the interfacial PMA energy by thermal annealing is not likely to be an intrinsic property of Fe/MgO but is caused by Fe-Cr intermixing, which results in hole doping in Fe from Cr atoms [39] and/or the formation of a Cr/MgO interface. On the possibility of enhancement of the PMA energy due to Fe-V intermixing, we have conducted similar experiments as Ref. [38] using V and confirmed that the Fe-V intermixing does not enhance the PMA energy. Therefore, while many reports on the enhancement of the PMA energy through annealing exist, we conclude that this energy is intrinsically insensitive to annealing in the Fe/MgO system. From the viewpoint of designing large PMA systems, relaxing epitaxial strain by thermal annealing is an effective strategy.

It has also been previously reported that the VCMA effect is insensitive to annealing [16–18]. Based on the earlier discussion on the PMA energy, the enhancement of the PMA energy by thermal annealing is not relevant to the modulation of the interfacial electronic states at the Fe/MgO interface, but can permit the relaxation of internal stress in the magnetic layer. Consequently, the VCMA effect, which is an electric field induced modulation of the interfacial PMA, is also insensitive to thermal annealing. Therefore, to obtain a system with a significant PMA and VCMA effects, the design of materials in which the local Fe-O hybridized orbitals at the Fe/MgO interface can be controlled is indispensable.

In conclusion, we studied the influence of epitaxial strain on the PMA energy in the Fe/MgO system. The modulation of the PMA energy mainly originates from the volume magnetic anisotropy due to the epitaxial strain. The interfacial PMA at the Fe/MgO interface is robust and largely unaffected by epitaxial strain and the annealing process. Our results provide a comprehensive understanding of PMA in ultrathin magnetic films and may lead to further developments in high PMA systems.

This work was partially supported by JSPS KAKENHI (Grant No. JP20K15158), JST-CREST (JPMJCR18T3), the JST-Mirai Program (JPMJMI20A1), and the Spintronics Research Network of Japan (Spin-RNJ). We thank T. Higo and S. Nakatsuji of the University of Tokyo for MOKE measurements. The XMCD experiment was done under the approval of the Photon Factory Program Advisory Committee (Proposal No. 2019S2-003).

[1] P. F. Carcia, A. D. Meinhaldt, and A. Suna, Perpendicular magnetic anisotropy in Pd/Co thin film layered structures, *Appl. Phys. Lett.* **47**, 178 (1985).
 [2] P. Bruno, Tight-binding approach to the orbital magnetic moment and magnetocrystalline anisotropy of transition-metal monolayer, *Phys. Rev B* **39**, 865 (1989).
 [3] J. Stöhr, Exploring the microscopic origin of the magnetic anisotropies with x-ray magnetic circular dichroism (XMCD) spectroscopy, *J. Magn. Magn. Mater.* **200**, 470 (1999).

[4] T. Shinjo, S. Hine, and T. Takada, Mössbauer spectra of ultrathin Fe films coated by MgO, *J. Phys., Colloq.* **40**, C2-86 (1979).
 [5] S. Yakata, H. Kubota, Y. Suzuki, K. Yakushiji, S. Yuasa, and K. Ando, Influence of perpendicular magnetic anisotropy on spin-transfer switching current in CoFeB/MgO/CoFeB magnetic tunnel junctions, *J. Appl. Phys.* **105**, 07D131 (2009).
 [6] S. Ikeda, K. Miura, H. Yamamoto, K. Mizunuma, H. D. Gan, M. Endo, S. Kanai, J. Hayakawa, F. Matsukura, and H. Ohno,

- A perpendicular-anisotropy CoFeB-MgO magnetic tunnel junction, *Nat. Mater.* **9**, 721 (2010).
- [7] H. Y. Yang, M. Chshiev, B. Dieny, J. H. Lee, A. Manchon, and K. H. Shin, First-principles investigation of very large perpendicular magnetic anisotropy at Fe/MgO and Co/MgO interface, *Phys. Rev. B* **84**, 054401 (2011).
- [8] C.-H. Lambert, A. Rajanikanth, T. Hauet, S. Mangin, E. E. Fullerton, and S. Andrieu, Quantifying perpendicular magnetic anisotropy at the Fe-MgO (001) interface, *Appl. Phys. Lett.* **102**, 122410 (2013).
- [9] J. W. Koo, S. Mitani, T. T. Sasaki, H. Sukegawa, Z. C. Wen, T. Ohkubo, T. Niizeki, K. Inomata, and K. Hono, Large perpendicular magnetic anisotropy at Fe/MgO interface, *Appl. Phys. Lett.* **103**, 192401 (2013).
- [10] B. Dieny and M. Chshiev, Perpendicular magnetic anisotropy at transition metal/oxide interface and applications, *Rev. Mod. Phys.* **89**, 025008 (2017).
- [11] S. Miwa, M. Suzuki, M. Tsujikawa, T. Nozaki, T. Nakamura, M. Shirai, S. Yuasa, and Y. Suzuki, Perpendicular magnetic anisotropy and its electric-field-induced change at metal-dielectric interfaces, *J. Phys. D: Appl. Phys.* **52**, 063001 (2019).
- [12] H. Cai, W. Kang, Y. Wang, L. A. De Barros Naviner, J. Yang, and W. Zhao, High performance MRAM with spin-transfer-torque and voltage-controlled magnetic anisotropy effects, *Appl. Sci.* **7**, 929 (2017).
- [13] S. Yuasa, T. Nagahama, A. Fukushima, Y. Suzuki, and K. Ando, Giant room-temperature magnetoresistance in single-crystal Fe/MgO/Fe magnetic tunnel junction, *Nat. Mater.* **3**, 868 (2004).
- [14] S. S. P. Parkin, C. Kaiser, A. Panchula, P. M. Rice, B. Hughes, M. Samant, and S.-H. Yang, Giant tunneling magnetoresistance at room temperature with MgO (100) tunnel barriers, *Nat. Mater.* **3**, 862 (2004).
- [15] D. D. Lam, F. Bonell, S. Miwa, Y. Shiota, K. Yakushiji, H. Kubota, T. Nozaki, A. Fukushima, S. Yuasa, and Y. Suzuki, MgO overlayer thickness dependence of perpendicular magnetic anisotropy in CoFeB thin films, *J. Korean Phys. Soc.* **62**, 1461 (2013).
- [16] W. Skowroński, T. Nozaki, D. D. Lam, Y. Shiota, K. Yakushiji, H. Kubota, A. Fukushima, S. Yuasa, and Y. Suzuki, Underlayer material influence on electric-field controlled perpendicular magnetic anisotropy in CoFeB/MgO magnetic tunnel junctions, *Phys. Rev. B* **91**, 184410 (2015).
- [17] Y. Shiota, T. Nozaki, S. Tamaru, K. Yakushiji, H. Kubota, A. Fukushima, S. Yuasa, and Y. Suzuki, Reduction in write error rate of voltage-driven dynamic magnetization switching by improving thermal stability factor, *Appl. Phys. Lett.* **111**, 022408 (2017).
- [18] J. Suwardy, K. Nawaoka, J. Cho, M. Goto, Y. Suzuki, and S. Miwa, Voltage-controlled magnetic anisotropy and voltage-induced Dzyaloshinskii-Moriya interaction change at the epitaxial Fe(001)/MgO(001) interface engineered by Co and Pd atomic-layer insertion, *Phys. Rev. B* **98**, 144432 (2018).
- [19] J. Sinha, M. Hayashi, A. J. Kellock, S. Fukami, M. Yamanouchi, H. Sato, S. Ikeda, S. Mitani, S.-H. Yang, S. S. P. Parkin, and H. Ohno, Enhanced interface perpendicular magnetic anisotropy in Ta[CoFeB]MgO using nitrogen doped Ta underlayers, *Appl. Phys. Lett.* **102**, 242405 (2013).
- [20] P. G. Growtham, G. M. Stiethl, D. C. Ralph, and R. A. Buhrman, Thickness-dependent magnetoelasticity and its effects on perpendicular magnetic anisotropy in Ta/CoFeB/MgO thin films, *Phys. Rev. B* **93**, 024404 (2016).
- [21] A. N. Anisimov, W. Platow, P. Pouloupoulos, W. Wisny, M. Farle, K. Baberschke, P. Isberg, B. Hjörvarsson, and R. Wäppling, The temperature-dependent in and out-of-plane magnetic anisotropy in Fe_n/V_m(001) superlattice, *J. Phys.: Condens. Matter* **9**, 10581 (1997).
- [22] A. N. Anisimov, W. Platow, P. Pouloupoulos, M. Farle, and K. Baderschke, P. Isberg, P. Granberg, and R. Wäppling, Magnetic anisotropies of Fe_n/V_m(001) superlattices determined by ferromagnetic resonance, *IEEE Trans. Magn.* **34**, 873 (1998).
- [23] A. Broddefalk, P. Nordblad, P. Blomquist, P. Isberg, R. Wäppling, O. Le Bacq, and O. Eriksson, In-plane magnetic anisotropy of Fe/V (001) superlattices, *J. Magn. Magn. Mater.* **241**, 260 (2002).
- [24] C. Liu, Y. Park, and S. D. Bager, Resistance minimum in ultrathin ferromagnetic films of Fe on MgO (100), *J. Magn. Magn. Mater.* **111**, L225 (1992).
- [25] Yu. V. Goryunov, N. N. Garif'yanov, G. G. Khaliullin, I. A. Garifullin, L. R. Tagirov, F. Schreiber, Th. Mühge, and H. Zabel, Magnetic anisotropies of sputtered Fe films on MgO substrates, *Phys. Rev. B* **52**, 13450 (1995).
- [26] S.-K. Lee, J.-S. Kim, B. Kim, Y. Cha, W. K. Han, H. G. Min, J. Seo, and S. C. Hong, Surface alloying and magnetism of ultrathin Fe films on Pd(001), *Phys. Rev. B* **65**, 014423 (2001).
- [27] F. Bonell, D. D. Lam, S. Yoshida, Y. T. Takahashi, Y. Shiota, S. Miwa, T. Nakamura, and Y. Suzuki, Investigation of Au and Ag segregation on Fe(001) with soft x-ray absorption, *Surf. Sci.* **616**, 125 (2013).
- [28] A. Koziol-Rachwał, T. Nozaki, V. Zayets, H. Kubota, A. Fukushima, S. Yuasa, and Y. Suzuki, The effect of the MgO buffer layer thickness on magnetic anisotropy in MgO/Fe/Cr/MgO buffer/MgO(001), *J. Appl. Phys.* **120**, 085303 (2016).
- [29] K. Amemiya, H. Kondoh, T. Yokoyama, and T. Ohta, A soft x-ray beamline for surface chemistry in the Photon Factory, *J. Electron Spectrosc. Relat. Phenom.* **124**, 151 (2002).
- [30] B. T. Thole, P. Carra, F. Sette, and G. van der Laan, X-Ray Circular Dichroism as a Probe of Orbital Magnetization, *Phys. Rev. Lett.* **68**, 1943 (1992).
- [31] P. Carra, B. T. Thole, M. Altarelli, and X. Wang, X-Ray Circular Dichroism and Local Magnetic Fields, *Phys. Rev. Lett.* **70**, 694 (1993).
- [32] Ch. Kittel, *Introduction to Solid State Physics*, 8th ed. (John Wiley, New York, 2005).
- [33] H. Matsumoto, S. Ota, T. Koyama, and D. Chiba, Control of magnetic anisotropy in a Co thin film on a flexible substrate by applying biaxial tensile strain, *Appl. Phys. Lett.* **118**, 022406 (2021).
- [34] S. V. Kaarthik, Y. K. Takahashi, T. Ohkubo, K. Hono, S. Ikeda, and H. Ohno, Transmission electron microscopy investigation of CoFeB/MgO/CoFeB pseudospin valves annealed at different temperature, *J. Appl. Phys.* **106**, 023920 (2009).
- [35] T. Miyajima, T. Ibusuki, S. Umehara, M. Sato, S. Eguchi, M. Tsukada, and Y. Kataoka, Transmission electron microscopy study on the crystallization and boron distribution of CoFeB/MgO/CoFeB magnetic tunnel junctions with various capping layers, *Appl. Phys. Lett.* **94**, 122501 (2009).

- [36] J. Okabayashi, J. W. Koo, H. Sukegawa, S. Mitani, Y. Takagi, and T. Yokoyama, Perpendicular magnetic anisotropy at the interface between ultrathin Fe film and MgO studied by angular-dependent x-ray magnetic circular dichroism, *Appl. Phys. Lett.* **105**, 122408 (2014).
- [37] T. Nozaki, A. Koziol-Rachwał, W. Skowroński, V. Zayets, Y. Shiota, S. Tamaru, H. Kubota, A. Fukushima, S. Yuasa, and Y. Suzuki, Large Voltage-Induced Changes in the Perpendicular Magnetic Anisotropy of an MgO-Based Tunnel Junction with an Ultrathin Fe Layer, *Phys. Rev. Appl.* **5**, 0444006 (2016).
- [38] A. Koziol-Rachwał, T. Nozaki, K. Freindl, J. Korecki, S. Yuasa, and Y. Suzuki, Enhancement of perpendicular magnetic anisotropy and its electric field-induced change through interface engineering in Cr/Fe/MgO, *Sci. Rep.* **7**, 5993 (2017).
- [39] J. Zhang, P. V. Lukashev, S. S. Jaswal, and E. Y. Tsymbal, Model of orbital populations for voltage-controlled magnetic anisotropy in transition-metal thin films, *Phys. Rev. B* **96**, 014435 (2017).

Correction: The given name of the third author contained an error and has been fixed.